NASA TECHNICAL MEMORANDUM

NASA TM-82394

THE PYROELECTRIC PROPERTIES OF TGS FOR APPLICATION IN INFRARED DETECTION

By R. L. Kroes and D. Reiss
Space Sciences Laboratory

January 1981

NASA

George C. Marshall Space Flight Center
Marshall Space Flight Center, Alabama

TECHNICAL REPORT STANDARD TITLE PAGE

1 REPORT NO.	2. GOVERNMENT ACCESSION NO.	3. RECIPIENT'S CATALOG NO.
NASA-82394		

4 TITLE AND SUBTITLE	5. REPORT DATE
The Pyroelectric Properties of TGS for Application in Infrared Detection	January 1981
	6. PERFORMING ORGANIZATION CODE
7. AUTHOR(S) R. L. Kroes and D. Reiss	8. PERFORMING ORGANIZATION REPORT #
9. PERFORMING ORGANIZATION NAME AND ADDRESS George C. Marshall Space Flight Center Marshall Space Flight Center, Alabama 35812	10. WORK UNIT NO.
	11. CONTRACT OR GRANT NO.
12 SPONSORING AGENCY NAME AND ADDRESS National Aeronautics and Space Administration Washington, D. C. 20546	13. TYPE OF REPORT & PERIOD COVERED Technical Memorandum
	14. SPONSORING AGENCY CODE

15 SUPPLEMENTARY NOTES
Prepared by Space Sciences Laboratory, Science and Engineering Directorate

16. ABSTRACT

This report describes the pyroelectric property of triglycine sulfate (TGS) and its application in the detection of infrared radiation. The detectivities of pyroelectric detectors and other types of infrared detectors are compared. The thermal response of a pyroelectric detector element and the resulting electrical response are derived in terms of the material parameters. The noise sources which limit the sensitivity of pyroelectric detectors are described, and the noise equivalent power for each noise source is given as a function of frequency and detector area.

17 KEY WORDS	18. DISTRIBUTION STATEMENT
	Unclassified–Unlimited

19 SECURITY CLASSIF. (of this report)	20 SECURITY CLASSIF. (of this page)	21 NO. OF PAGES	22 PRICE
Unclassified	Unclassified	35	NTIS

TABLE OF CONTENTS

LIST OF ILLUSTRATIONS

TECHNICAL MEMORANDUM

THE PYROELECTRIC PROPERTIES OF TGS FOR APPLICATION IN INFRARED DETECTION

INTRODUCTION

There are two methods by which infrared radiation can be detected. These are (1) the direct detection of incident photons and (2) the detection of the increase in temperature of a material resulting from the absorption of radiation. In this report we will direct our attention to infrared radiation detection utilizing the pyroelectric property of triglycine sulfate $(NH_2CH_2COOH)_3$ (H_2SO_4), usually abbreviated TGS [1]. But, first, as a means of comparison, we will give a brief general description of infrared detectors.

Photon detectors are classified according to their mode of operation as either photovoltaic or photoresistive. In these detectors made of semiconductor material, incident photons which are of sufficient energy interact with the material to excite charge carriers between valence and conduction bands (intrinsic detectors) or between impurity states and one of the bands (extrinsic detectors). The major effort in developing these detectors over the past several decades has been to extend their long wavelength threshold so that they would respond in the 3 to 5 micron and 8 to 14 micron atmospheric windows (Fig. 1) [2,3]. One property of these detectors to keep in mind is that for optimum operation they need to be cryogenically cooled. In some applications this can be a serious disadvantage.

Thermal detectors are based on a variety of temperature-dependent properties, such as: the voltage generated when a junction between unlike metals is heated (thermocouple), the change in resistance of a metal or semiconductor (bolometer), the change in pressure of an enclosed gas (Golay cell), or the change in polarization of certain dielectric materials (pyroelectric detector) [4]. One advantage these detectors have over photon detectors is that they respond uniformly over a wide spectral region if they possess a surface absorption layer which is wavelength invariant. On the other hand, they are generally less sensitive (Fig. 2).

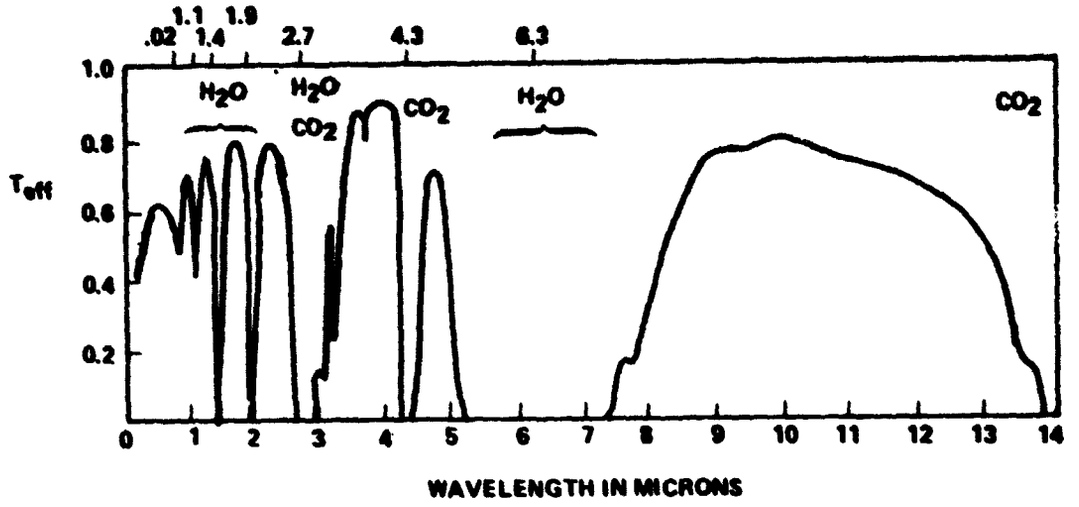

Figure 1. Spectral transmittance of 2000 yards of sea-level atmosphere at low humidity and low haziness [3].

PYROELECTRIC MATERIALS

Crystals are commonly classified according to their geometric structure into seven systems: triclinic, monoclinic, orthorhombic, tetragonal, trigonal, hexagonal, and cubic. These seven systems can be subdivided into 32 crystal point groups according to their symmetry with respect to a point [5]. Of these 32 crystal point groups, 11 are centrosymmetric (possessing a center of symmetry) and are not electrically polarized when subjected to a uniform stress. The remaining 21 crystal classes are noncentrosymmetric, and 20 of these become electrically polarized when subjected to an applied stress. This property is called the piezoelectric effect[1]. Piezoelectricity is determined solely by the crystal symmetry. Thus, if a crystal belongs to one of the preceding 20 noncentrosymmetric classes, it will be piezoelectric.

The pyroelectric materials form a subgroup (containing 10 crystal classes) of the piezoelectrics (see Appendix A) [7, 8]. They possess a spontaneous electrical polarization. This polarization is usually masked by stray charges from the atmosphere which collect on the surface and tend to neutralize it. However, when the temperature of such a crystal is altered, the polarization changes; this change can be observed, hence

1. Piezoelectricity is the electric polarization produced by an applied stress. This effect was discovered by J. Curie and P. Curie in 1880 when they realized that the difference between the charge developed upon uniform and nonuniform heating was due to the thermal stress created in the pyroelectric sample [6].

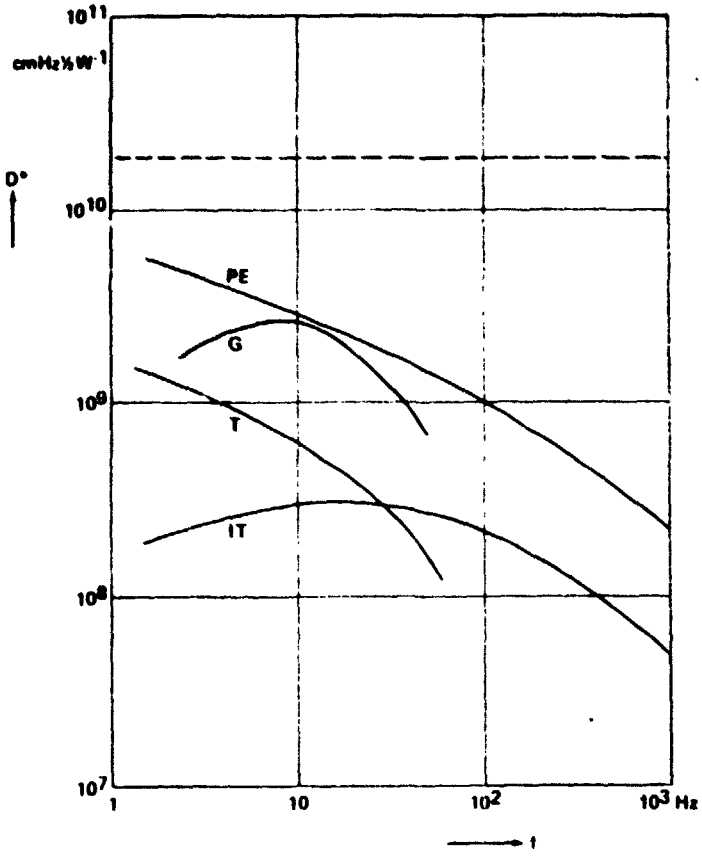

Figure 2. The area-normalized detectivity as a function of frequency for various types of thermal detectors: the pyroelectric element (PE), the Golay cell (G), the thermopile (T), and an immersed thermistor (IT). The dashed line represents the limiting case of the ideal thermal detector.

the name pyroelectric. Pyroelectricity, like piezoelectricity, is solely a property of crystal symmetry. Hence, any crystal belonging to one of the 10 pyroelectric crystal classes will have the pyroelectric property. It has been found that most of the pyroelectrics which possess the largest pyroelectric coefficients also belong to the relatively small class of materials called ferroelectrics. These materials typically have a pyroelectric coefficient 10 to 100 times greater than nonferroelectric pyroelectrics.

The ferroelectrics form a subgroup of the pyroelectrics [9]. They possess spontaneous electrical polarization, like the pyroelectrics, but have the additional property that their polarization can be reversed by an applied electric field. They exhibit an electric hysteresis analogous to the magnetic hysteresis exhibited by ferromagnets (Fig. 3). This additional property cannot be predicted from crystal structure alone but must be determined on an experimental basis. Associated with each

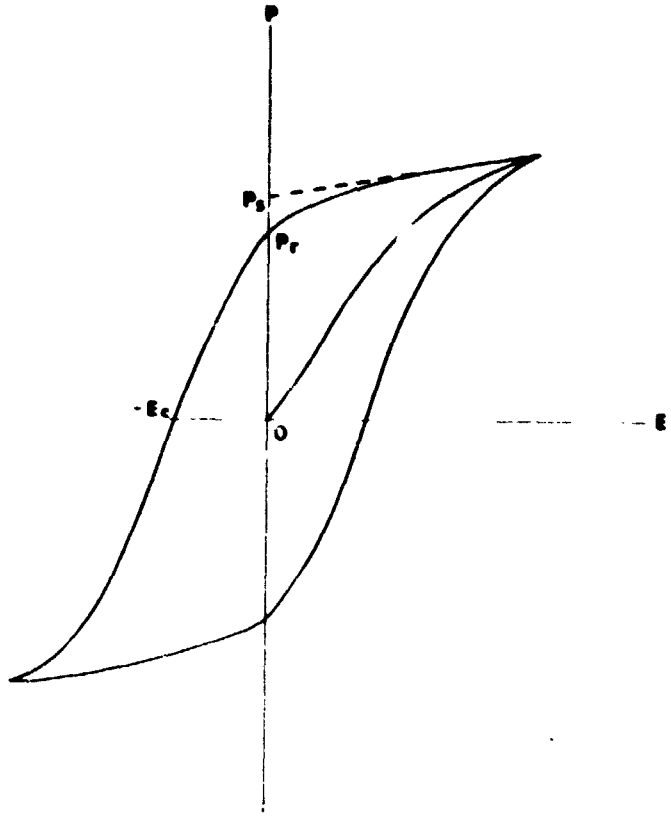

Figure 3. Ferroelectric hysteresis.

ferroelectric is a critical temperature called the Curie temperature. Above this temperature the ferroelectric property disappears. Below the Curie temperature, a ferroelectric usually consists of a number of oppositely polarized domains. To give the crystal a unique sense of polarization, an external electric field must be applied to align all the domains. This is known as "poling" the crystal [10]. When the external field is removed, as is required to achieve low noise performance for infrared detection, new domains of opposite polarization may appear at a later time, resulting in a reduction of detector signal.

TGS is a ferroelectric with a Curie temperature of 49°C. It has a monoclinic crystal structure with a space group of P2 below the Curie temperature. Its pyroelectric coefficient goes to zero as the Curie temperature is reached; therefore, as an infrared detector it must be used below 49°C. Figure 4 shows the temperature dependence of its polarization, pyroelectric coefficient and dielectric constant [11]. The best compromise between performance, resistance to depoling, and reasonable temperature range of operation is achieved when TGS is used at or near room temperature. TGS is water soluble, and single crystals can readily be grown from an aqueous solution. It has a single cleavage axis perpendicular to its pyroelectric axis and is sometimes grown from a deuterated solution or one containing ℓ-alanine [12, 13].

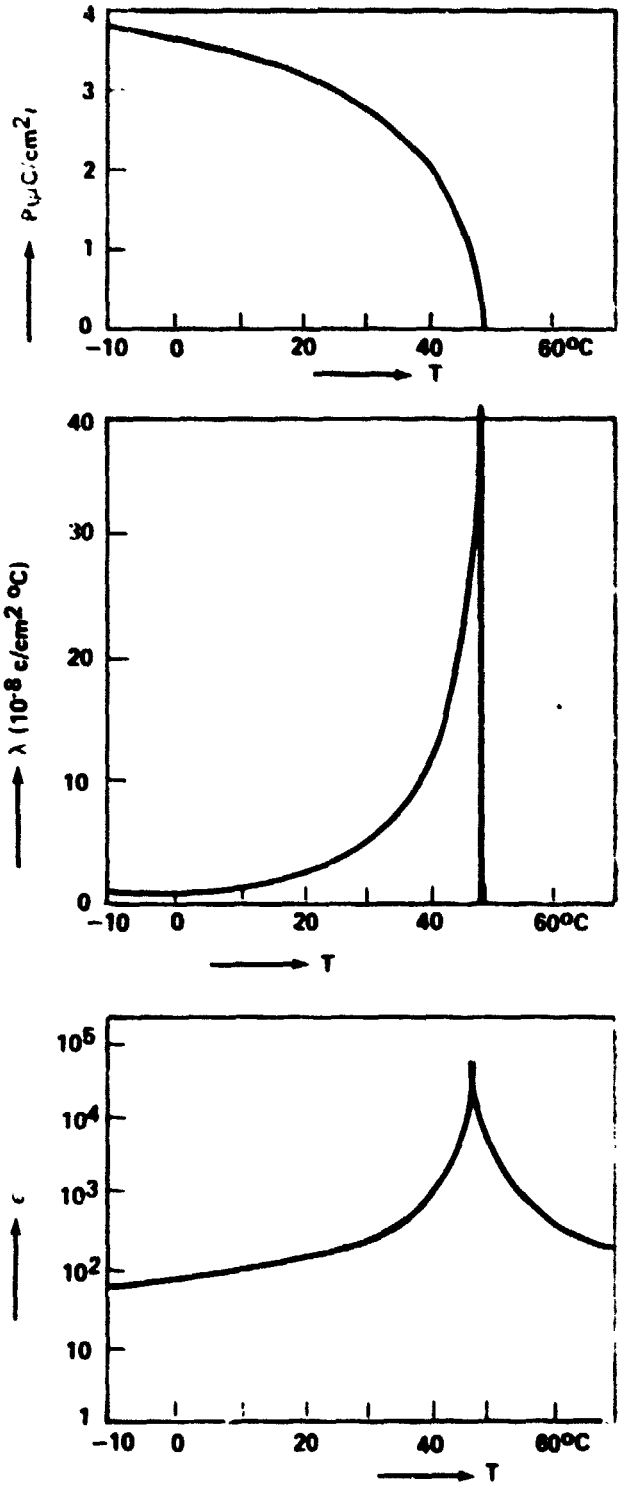

Figure 4. The temperature dependence of the polarization P, the pyroelectric coefficient λ and the dielectric constant ε for a crystal of pure TGS ($\lambda = dP/dT$).

PYROELECTRIC INFRARED DETECTION

A pyroelectric infrared detector may be made by applying electrodes to those surfaces of a plate of pyroelectric material normal to the axis of polarization. Infrared radiation incident on the detector is absorbed and changed to heat, causing the temperature of the plate to rise. A change in the spontaneous polarization (P) of the plate proportional to the change in temperature (T) is produced:

$$dP = \lambda dT \quad . \tag{1}$$

The constant, λ, is called the pyroelectric coefficient. If the electrodes are connected through an external circuit, a current will flow until the polarization surface charge $\sigma = \vec{P} \cdot \hat{n}$ is compensated by free charges flowing in the circuit. This current is given by

$$i = A \frac{d\sigma_p}{dt} = A \frac{dP}{dt} = A \frac{dP}{dT} \frac{dT}{dt} = A \lambda \frac{dT}{dt} \tag{2}$$

where A is the area of the electroded crystal surface. The current is a measure of the rate of change of the temperature of the detector and is, therefore, a measure of the incident radiation.

Because the current is proportional to the time rate of change of detector temperature, a constant infrared radiation input to the detector will generate no signal once the detector has reached thermal equilibrium. Therefore, an optical chopper must be used ahead of the detector.[2] If the incident radiation is chopped at a frequency ω, the detector will respond as shown qualitatively in Figure 5.

To obtain a quantitative result we will use the method illustrated in Figure 6.

If the detector is originally at the temperature of its surroundings (heat sink), T, the absorption of the incident radiation will raise it to a temperature $T + \theta$. It will then lose heat to its surroundings at a rate $G\theta$. The heat rate balance equation can then be written as:

$$\eta W = H \frac{d\theta}{dt} + G\theta \tag{3}$$

2. Pyroelectric detectors may also be used without choppers to detect transient signals, such as laser pulses. In this mode they can measure the total energy of the transient by storing the total electrical surface charge liberated by the signal [8].

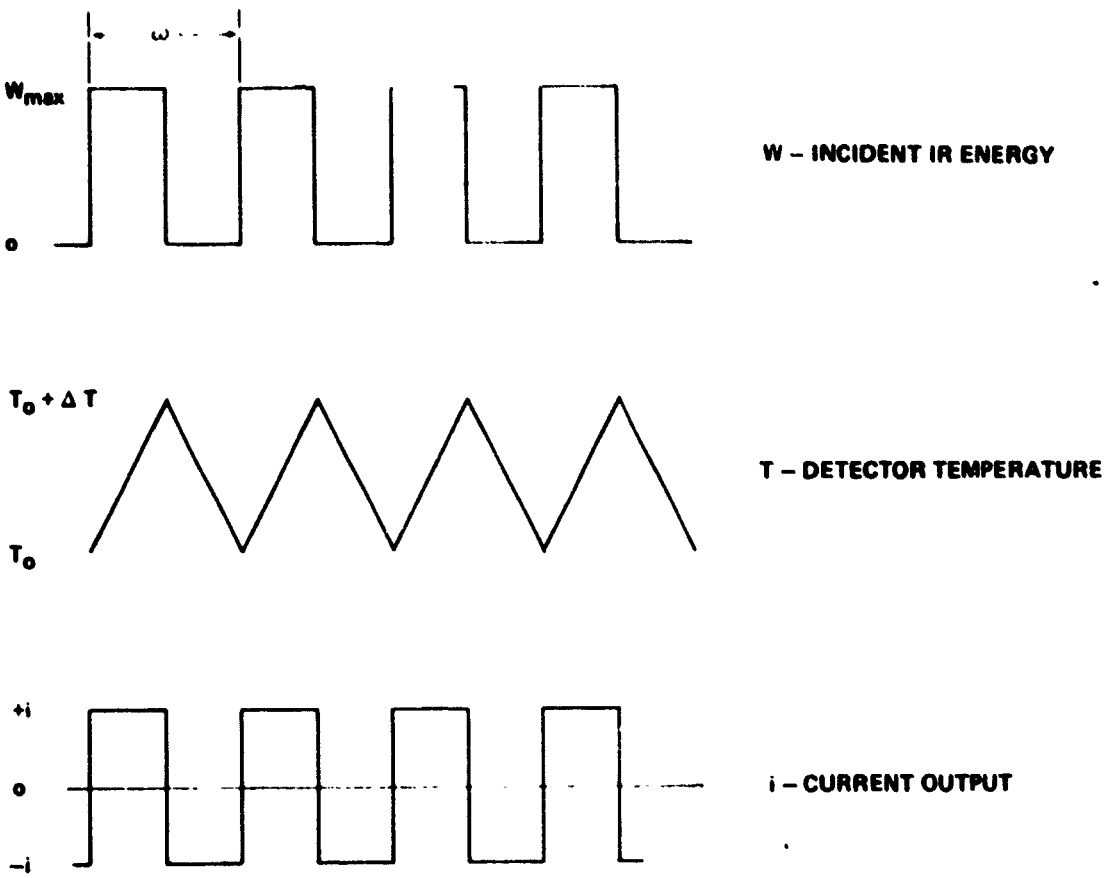

Figure 5. Thermal and electrical response of a pyroelectric detector to chopped infrared radiation.

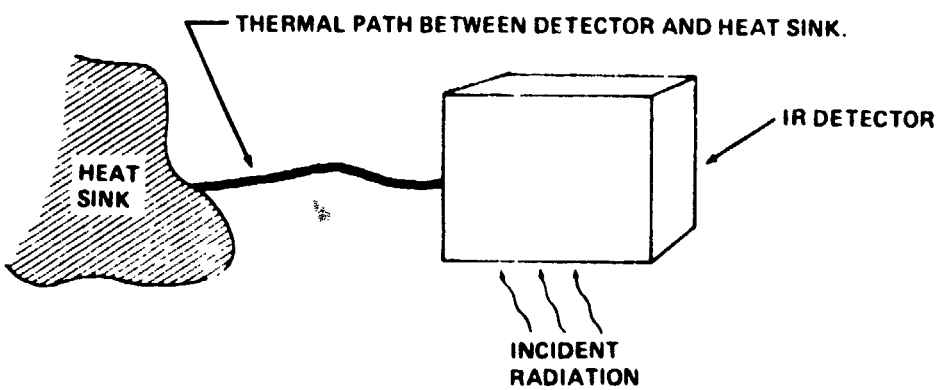

Figure 6. Equivalent thermal circuit of a pyroelectric detector.

where:

η is the emissivity of the detector surface

W is the incident radiation power

H is the thermal mass of the detector

G is the thermal conductance between the detector and its heat sink

$\theta = T_d - T$ is the difference in temperature between the detector (T_d) and the heat sink (T).

The limiting value of G is the radiative conductance for each radiating surface

$$G_r = 4 \sigma \eta A \theta^3 \qquad (4)$$

where σ is the Stefan-Boltzmann constant, η is the emissivity of the surface, and A is the area of the surface. In an actual detector there will usually be other significant contributions to the conductance. The power incident on a thin slab of pyroelectric material from a beam of infrared radiation chopped at a frequency ω can be expressed as:

$$W = W_o (1 - e^{i\omega t}) \quad . \qquad (5)$$

If equation (5) is substituted into equation (3) and the differential equation solved for θ, we get a transient term plus a steady state solution consisting of an average temperature change of

$$\theta_{av} = \eta W_o / G \quad , \qquad (6)$$

and oscillating component

$$\theta_\omega = [\eta W_o / (G^2 + \omega^2 H^2)^{1/2}] \, e^{i(\omega t + \phi)} \qquad (7)$$

where the phase angle is $\phi = \tan^{-1} (\omega H/G)$ (see Appendix B). This is the phase difference between the incident radiation and the temperature response. For maximum thermal response to a given incident radiation it is clear from equation (7) that the value of G should be as small as

possible and ω sufficiently small so that $\omega H << G$. That is to say, we want to maximize the interaction of the thermal detector with regard to the incident radiation (H small) while minimizing as far as possible all other thermal contacts of the detector with its surroundings (G small). It is also clear that as ω increases, the term $\omega^2 H^2$ will eventually become greater than G^2. When this happens, the temperature response θ_ω will start to decrease inversely as ω. This defines a characteristic thermal time constant $\tau_T = H/G$. Generally τ_T will have a value in the range of tens of milliseconds to seconds. It is a measure of how quickly the detector responds thermally to the onset of incident radiation [14]. These general characteristics are shown in Figure 7. The calculations in equations (3) through (7) assume that the incident radiation is absorbed uniformly throughout the sample. This may not be entirely correct if the material has a large absorption coefficient or if it is coated with a thin absorbing layer.

One way of electrically describing a pyroelectric detector is shown in Figure 8. Here the detector is represented by a current source in parallel with the detector's capacitive (C_E) and resistive (R_E) output impedance. The output from this detector is fed into an amplifier whose input impedance is also shown schematically in Figure 8. The voltage applied to the amplifier is the voltage across the combined impedances of the detector and the amplifier [15, 16].

$$V = i \mid Z \mid = i R (1 + \omega^2 \tau_E^2)^{-1/2} \qquad (8)$$

where

$$\frac{1}{R} = \frac{1}{R_E} + \frac{1}{R_A} \quad \text{and} \quad C = C_E + C_A \quad .$$

Here $\tau_E = RC$ is the electrical time constant of the combined impedances, and

$$i = \lambda A \, d\theta/dt = \lambda A \omega \theta_\omega \quad . \qquad (9)$$

Therefore,

$$V = \omega \lambda A \, \theta_\omega R (1 + \omega^2 \tau_E^2)^{-1/2} \quad , \qquad (10)$$

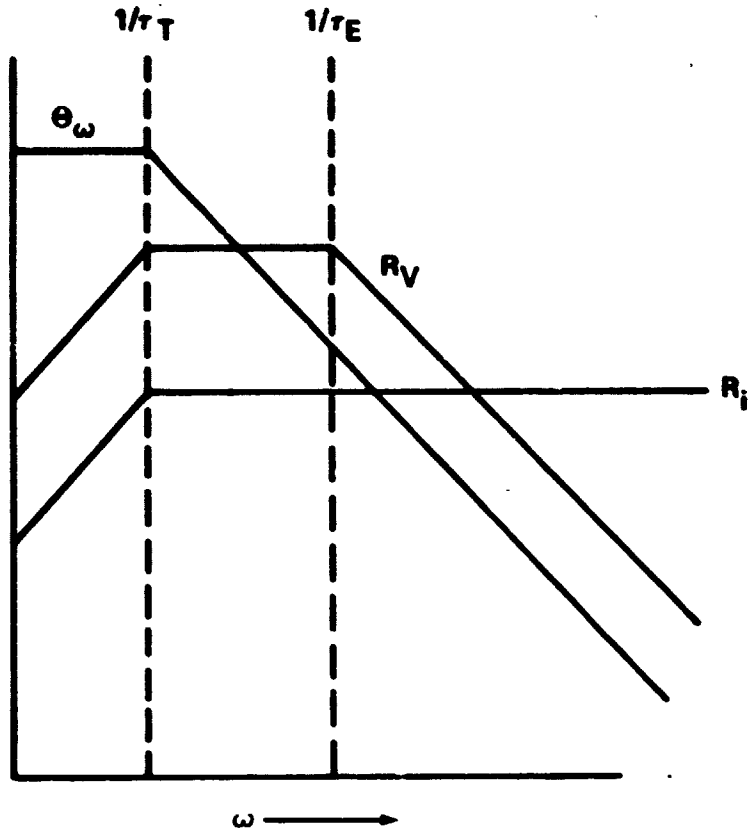

Figure 7. The thermal response (Θ_ω) and the voltage (R_V) and current (R_i) responsivities of a pyroelectric detector as a function of frequency. τ_T and τ_E are the thermal and electrical time constants of the detector.

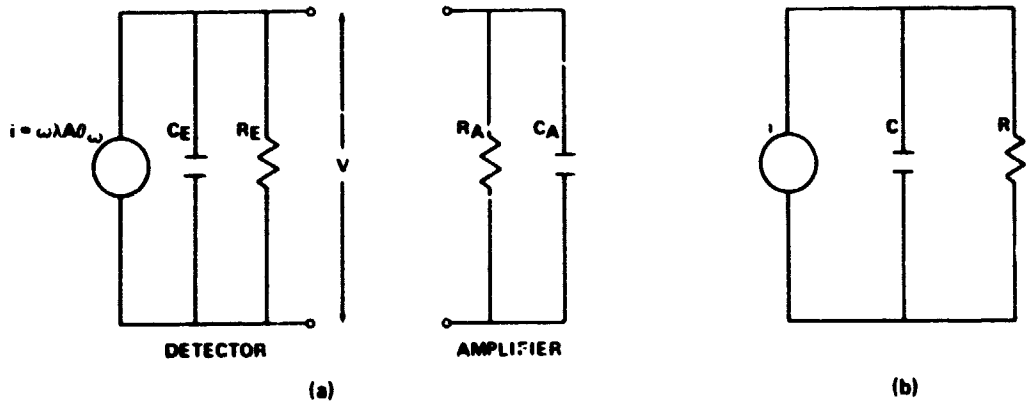

Figure 8. Equivalent circuits for a pyroelectric detector. (a) Equivalent circuits of a pyroelectric element and an amplifier. (b) Equivalent circuit showing the combined impedance of the detector element and the amplifier.

but,

$$\theta_\omega = \eta W_o (G^2 + \omega^2 H^2)^{-1/2} = (\eta W_o/G) (1 + \omega^2 \tau_T^2)^{-1/2} \quad ; \tag{11}$$

hence,

$$V = \omega \lambda AR (\eta W_o/G) (1 + \omega^2 \tau_T^2)^{-1/2} (1 + \omega^2 \tau_E^2)^{-1/2} \quad . \tag{12}$$

The voltage responsivity is defined as the output voltage/input radiant power:

$$R_V = V/W = (\eta \omega \lambda AR/G) (1 + \omega^2 \tau_T^2)^{-1/2} (1 + \omega^2 \tau_E^2)^{-1/2} \quad . \tag{13}$$

Similarly, the current responsivity is defined as output current/input radiant power:

$$R_i = i/W = (\eta \omega \lambda A/G) (1 + \omega^2 \tau_T^2)^{-1/2} \quad . \tag{14}$$

The responsivity reaches its greatest value at chopping frequencies greater than the thermal relaxation frequency, G/H, which falls typically within the range 0.1 to 10 Hz, depending on the thickness of the crystal plate and the method of mounting. A typical detector made from a TGS plate 1 mm square and 20 μm thick will have a thermal relaxation frequency $f_T = 0.8$ Hz [7]. Chopping frequencies greater than 10 Hz are used in the majority of applications; therefore, the high frequency approximations of equations (11) through (13) may be used.

$$\theta_\omega \simeq \eta W/\omega H \tag{15}$$

$$R_V \simeq \eta \lambda A/\omega HC \quad . \tag{16}$$

In terms of material parameters,

$$R_V \simeq (1/\omega\varepsilon_o) (\eta \lambda/\varepsilon C_p) (1/A) \tag{17}$$

where ϵ_o is the permittivity of free space, ϵ is the dielectric constant, and c_p is the volume specific heat.

PERFORMANCE OF PYROELECTRIC DETECTORS

One of the important performance parameters for any infrared detector is its ultimate sensitivity. For a pyroelectric detector this ultimate sensitivity is expressed by the noise equivalent power (NEP), which is defined as the minimum detectable power per unit frequency bandwidth at a given operating frequency and radiation wavelength. The more sensitive the detector, the lower its NEP. The units for NEP are $W/Hz^{1/2}$.

The ultimate limit of the sensitivity for the detector is determined by the presence of noise signals generated within the detector element and its associated electronics [18-20]. The principal noise sources are: (1) temperature or radiation noise, (2) Johnson noise, (3) amplifier current noise, and (4) amplifier voltage noise.

Temperature or Radiation Noise

When thermal equilibrium has been established between a small body of thermal capacity H and a heat sink at temperature T through a thermal conductance G, there will be no mean power flow between the body and the sink. However, there will still exist power fluctuations whose rms value is given by

$$\Delta W_T = [4\ k\ TG^2\ (\Delta f)]^{1/2} \qquad (18)$$

where

ΔW_T = thermal energy fluctuation

$k = 1.38 \times 10^{-23}\ JK^{-1}$ Boltzmann's constant

T (°K) = temperature

G = thermal conductance

Δf = the frequency bandwidth.

These power fluctuations will be minimal when G is a minimum. This occurs when the only thermal coupling between the detector and its heat sink is via radiative exchange. Applying the Stefan-Boltzmann radiation law, the radiative thermal conductance is

$$G_R = 4 A \eta \sigma T^3 \qquad (19)$$

where

A = area of the detector

η = emissivity

σ = Stefan-Boltzmann's constant

T = temperature,

for a single radiating surface of area A. For a thin plate with both sides at the same temperature, T, the value of G_R will be doubled.

Johnson Noise

In a resistor the random thermal motion of free electrons will cause random positive and negative voltages to appear. This is the origin of Johnson noise in a resistor, and the resultant rms noise voltage so generated is given by:

$$\Delta V_J = [4 k T R (\Delta f)]^{1/2} \qquad (20)$$

where k is the Boltzmann constant, T is the temperature, R is the resistance, and Δf is the frequency bandwidth.

To understand the origin of Johnson noise in the pyroelectric detector element one must first realize that it is not a perfect or ideal capacitor. An ideal capacitor is one in which no energy is irreversibly dissipated during a complete charge-discharge cycle. There are two mechanisms for irreversible energy dissipation in real capacitors:

1) The dielectric is not a perfect insulator, and some free charge carriers will move through the dielectric from one plate to the other under an applied field. The random thermal motion of these free charge carriers causes a Johnson noise voltage to appear across the element.

2) Some energy is irreversibly lost in the polarization reversal process. The measure of this loss is given by the dielectric loss tangent.

Because of these properties, the dielectric element is represented by the electrically equivalent circuit of a capacitor C_E and a resistor R_E in parallel. Also note that the input impedance of the amplifier is also represented by a resistor R_A and a capacitor C_A in parallel as in Figure 8.

If we use the preceding description of the detector plus the amplifier input impedance, then in calculating the Johnson noise generated by it we must replace R in equation (20) by the impedance of the circuit shown in Figure 8. This gives

$$\Delta V_J = [4\ k\ T\ |\ Z\ |\ (\Delta f)]^{1/2} = \left[4\ k\ T\ \frac{R}{1 + \omega^2\ R^2\ C^2}\ \Delta f\right]^{1/2} . \tag{21}$$

For frequencies such that $\omega^2\ R^2\ C^2 \gg 1$ we get

$$\Delta V_J = \frac{(4\ k\ T\ \Delta f)^{1/2}\ R^{-1/2}}{\omega C} . \tag{22}$$

Recall that the voltage responsivity is

$$R_V = \frac{\eta\ (\omega\lambda\ AR/G)}{(1 + \omega^2\ R^2\ C^2)^{1/2}\ (1 + \omega^2\ H^2/G^2)^{1/2}} + \frac{\eta\ \lambda\ A}{\omega H\ C} \tag{23}$$

for frequencies such that $\omega R^2\ C^2 \gg 1$ and $\omega^2\ H^2/G^2 \gg 1$. Then the incident power required to generate a signal voltage equal to the Johnson noise voltage is given by

$$P = \frac{\Delta V_J}{V} = \frac{(4\ k\ T\ \Delta f)^{1/2}\ R^{-1/2}}{\eta\lambda A/\omega HC} , \tag{24}$$

which becomes

$$P = \frac{[4\ k\ T\ (\Delta f)]^{1/2}}{\eta\lambda}\ C_p\ (aA)^{1/2}\ \omega^{1/2} \tag{25}$$

where

$$H = C_p \, aA \text{ and } \sigma = \frac{1}{R} \frac{a}{A} \quad .$$

One must understand that the conductivity σ in equation (25) should include both the dc conductivity and the dielectric loss $\omega\varepsilon''$ of the material.

Amplifier Current Noise

This type of noise is caused by fluctuations in the current arising from the discrete nature of charge carriers. In bipolar transistors the noise originates in the base current. In JFET's the gate leakage current, which is very small, is the source of current noise. The rms noise current for a 1 Hz bandwidth is

$$\Delta i_A = (2 \, ei)^{1/2} \qquad (26)$$

where i is the current and e is the electronic charge. The equivalent noise voltage is

$$\Delta V_i = R \Delta i_A \, (1 + \omega^2 \, \tau_E^{\,2})^{-1/2} \quad . \qquad (27)$$

At high frequencies this becomes

$$\Delta V_i = \Delta i_A / \omega C = (2 \, ei)^{1/2} / \omega C \quad . \qquad (28)$$

Amplifier Voltage Noise, V_A

This is a noise voltage produced by the amplifier, which may be observed when the amplifier input is short-circuited. It is independent of the impedance of the circuit connected to the input of the amplifier. It has been measured on several amplifiers and has been observed to decrease as $1/f^{1/4}$ until becoming independent of frequency in the range of 500 to 5000 Hz [17].

The four noise voltages can be replaced by an equivalent noise voltage

$$\Delta V_N = (\Delta V_T^2 + \Delta V_J^2 + \Delta V_i^2 + \Delta V_A^2)^{1/2} \quad . \tag{29}$$

A minimum detectable incident power, P_N, can now be defined in the following manner: consider an incident (rms) power signal, P_N, which produces a (rms) signal voltage, V_S, which is just equal to ΔV_N, with an amplifier bandwidth Δf. Then

$$P_N R_V = V_S = \Delta V_N \quad , \tag{30}$$

so

$$P_N = \frac{\Delta V_N}{R_V} \quad . \tag{31}$$

Similarly, one can define the NEP as the minimum detectable power per unit frequency bandwidth at a given operating frequency and incident radiation wavelength,

$$NEP = \frac{P_N}{(\Delta f)^{1/2}} = \frac{\Delta V_N}{(\Delta f)^{1/2} R_V} \ WHz^{-1/2} \quad . \tag{32}$$

The minimum power of a detector is often described by the detectivity, which is the reciprocal of the NEP;

$$D = 1/NEP \ Hz^{1/2} \ W^{-1} \quad . \tag{33}$$

Since the intensities of some of the noise sources are proportional to the square root of the detector area, a figure of merit often used to compare the performances of detectors is the area normalized detectivity

$$D^* = A^{1/2}/NEP \ cm \ Hz^{1/2} \ W^{-1} \quad . \tag{34}$$

The wavelength or black body temperature of radiation used, the chopping frequency, and the amplifier bandwidth are normally specified with the detectivities.

In discussions about the ultimate sensitivity of thermal detectors, one often comes across the term "ideal thermal detector." By this is meant one in which the NEP is limited solely by the temperature noise and in which the Johnson noise, amplifier current, and voltage noises are assumed to be zero. In this limiting case the NEP is just equal to the thermal noise. Thus, from equation (18) we have

$$NEP = [4kT^2G]^{1/2} \quad , \tag{35}$$

and for a minimal value,

$$G = G_R = 8\,A\,\eta\,\sigma\,T^3$$

where it is assumed that both sides of the detector are radiating. Hence,

$$NEP = [32\,A\,\eta\,\sigma\,kT^5]^{1/2} \tag{36}$$

where $\sigma = 5.67 \times 10^{-12}$ J cm^{-2} K^{-4} and $k = 1.38 \times 10^{-23}$ J K^{-1}. Setting $A = 1$ cm^2, $T = 300^\circ$K and $\eta = 1$; completing the calculation gives

$$NEP = 7.8 \times 10^{-11}\ W\ H_z^{-1/2} \tag{37}$$

or

$$D^* = A^{1/2}/NEP = 1.3 \times 10^{10}\ cm\ W^{-1}\ Hz^{1/2} \quad . \tag{38}$$

In the case of real pyroelectric detectors the Johnson noise, amplifier current, and amplifier voltage noises cannot be ignored and, in fact, are the real limiting factors in determining the total NEP. This can be illustrated by the following expressions for the NEP due to each of the noise sources when using the high frequency approximation:

$$P_{N\ \text{Temperature}} = \Delta V_T/R_V = [16\ \eta\ \sigma\ kT]^{1/2}\ A^{1/2} \qquad (39)$$

$$P_{N\ \text{Johnson}} = \Delta V_J/R_V = [(4kT)^{1/2}/\eta\lambda]\ \sigma^{1/2}\ C_p\ (aA)^{1/2}$$

$$= [(4kT)^{1/2}/\eta\lambda]\ C_p\ (aA)^{1/2}\ (\omega\varepsilon'')^{1/2} \qquad (40)$$

$$= [(4kT)^{1/2}/\eta\lambda]\ C_p\ (aA)^{1/2}\ (\omega\varepsilon'\ \tan\ \delta)^{1/2} \qquad (41)$$

$$P_{N\ \text{Amp. Current}} = \Delta V_i/R_V = \Delta i\ C_p\ a/\eta\lambda \qquad (42)$$

$$P_{N\ \text{Amp. Voltage}} = \Delta V_A/R_V = \Delta V_A\ \omega\ C_p\ A_c/\eta\lambda \quad . \qquad (43)$$

These expressions lead to the general character log-log plot of NEP versus frequency shown in Figure 9 [21].

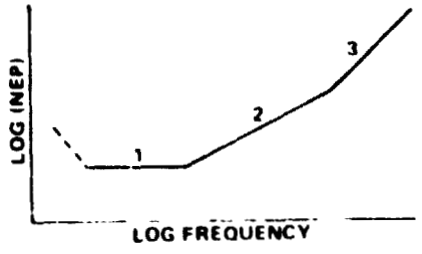

Figure 9. Variation of noise equivalent power with frequency.

The dominant noise source for each frequency region is as follows:

1) Region 1 due to amplifier current noise (NEP independent of ω)

2) Region 2 due to Johnson noise (NEP $\alpha\ \sqrt{\omega}$)

3) Region 3 due to amplifier voltage noise (NEP $\alpha\ \omega$).

It should be noted that the NEP due to temperature noise is not shown in Figure 9 because it is of smaller magnitude than the others, and it is also independent of frequency.

The effect of the area of the detector on the NEP can also be seen in Figure 10.

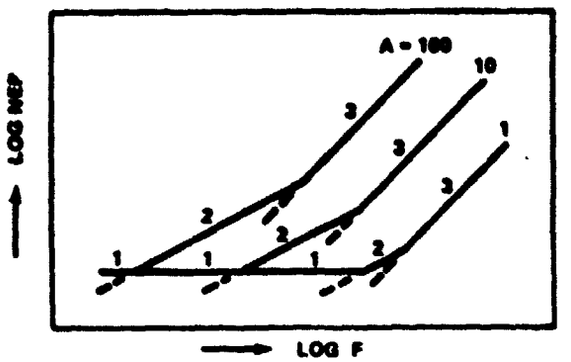

Figure 10. Noise equivalent power NEP versus frequency F for three values of the electrode area A.

To express the properties required to minimize the NEP, some attempts have been made to define a figure of merit for pyroelectric detectors. Unfortunately, no single combination of parameters will suffice for all operating circumstances; thus, the following three figures of merit are sometimes used [11]: (1) λ/C_p for low frequencies and small areas, (2) $\lambda p^{1/2}/C_p$ for intermediate frequencies and areas, and (3) $\lambda/C_p\varepsilon$ for high frequencies and large areas.

To illustrate the effects of detector configuration on detectivity, we can consider a detector using a single TGS element with a voltage mode FET amplifier. The FET is a 2N4861 JFET which has been selected for the lowest noise levels. The material properties of TGS and the pertinent parameters of the JFET are given in Table 1. (A wide range of values for some of these parameters is found in the literature; these are typical values.)

TABLE 1

Properties of TGS at 25° C [17]
$\lambda = 4.0 \times 10^{-8}$ C cm^{-2} K^{-1}
Dielectric constant $\varepsilon = 35$
Volume resistivity $\rho = 1.7 \times 10^{10}$ Ωcm
Volume heat capacity c' = 2.5 J cm^{-3} K^{-1}
Emissivity $\eta = 1$ (assumed)
JFET Characteristics (Selected 2N4861) [22]
Voltage noise at 25° C, 100 Hz, $e_n \sim 3$ nV/$\sqrt{\text{Hz}}$
Gate leakage current at 25° C, $I_G \sim 1$ p A
Voltage noise at -100° C, 100 Hz, $e_n \sim 1.5$ nV/$\sqrt{\text{Hz}}$
Gate leakage current at -100° C, $I_G \sim 0.01$ p A

This detector will use a chopper frequency of 100 Hz. The thickness of the TGS element will be 20 μm. Using equations (39) through (43) we can calculate the NEP of each noise source.

For this detector, the values of NEP at T = 25° C are

$$NEP_{\Delta V_i} = 7 \times 10^{-11} \text{ W } H_z^{-1/2}$$

$$NEP_{\Delta V_A} = 3.65 \times 10^{-12} \text{ A W Hz}^{-1/2}$$

$$NEP_{\Delta W_T} = 7.67 \times 10^{-11} \text{ A}^{1/2} \text{ W Hz}^{-1/2} \quad ,$$

$$NEP_{\Delta V_J} = 2.75 \times 10^{-9} \text{ A}^{1/2} \text{ W Hz}^{-1/2} \quad ,$$

where A is detector area, and assuming load resistance $R_L = 10^{11}\ \Omega$.

The values of NEP as a function of area are shown in Figure 11. The dependence of the NEP on area shows that detector geometry will determine which noise source is dominant. This provides a method of optimizing detector performance. There are two possible configurations for a pyroelectric detector: the face electrode, in which the pyroelectric axis is normal to the receiving area and a transparent or absorbing electrode is applied to the front surface of the detector, and the edge electrode, in which the pyroelectric axis is parallel to the receiving area and the electrodes are applied to the edges of the plate. These configurations are shown in Figure 12.

The values of NEP calculated previously were for the face electrode configuration. In calculating NEP for the edge electrode configuration the area of the receiving surface and the area of the electrodes are not the same. In calculating the temperature noise the receiving area A_r is used, while the electrode area A_e is used for Johnson and amplifier voltage noise. $NEP\Delta W_T$ is the same for both configurations. $NEP\Delta V_j$ involves the value Ad. d is the distance between electrodes. which is the plate thickness in the face configuration and the length of a side in the edge configuration. Therefore, Ad is the same value for both configurations, so Johnson noise does not depend on geometry. However, the responsivity depends on A, so the relative importance of amplifier noise is affected by geometry. For the edge electrode, $NEP\Delta V_i$ will be larger and $NEP\Delta V_A$ will be smaller than for the face electrode configuration [14].

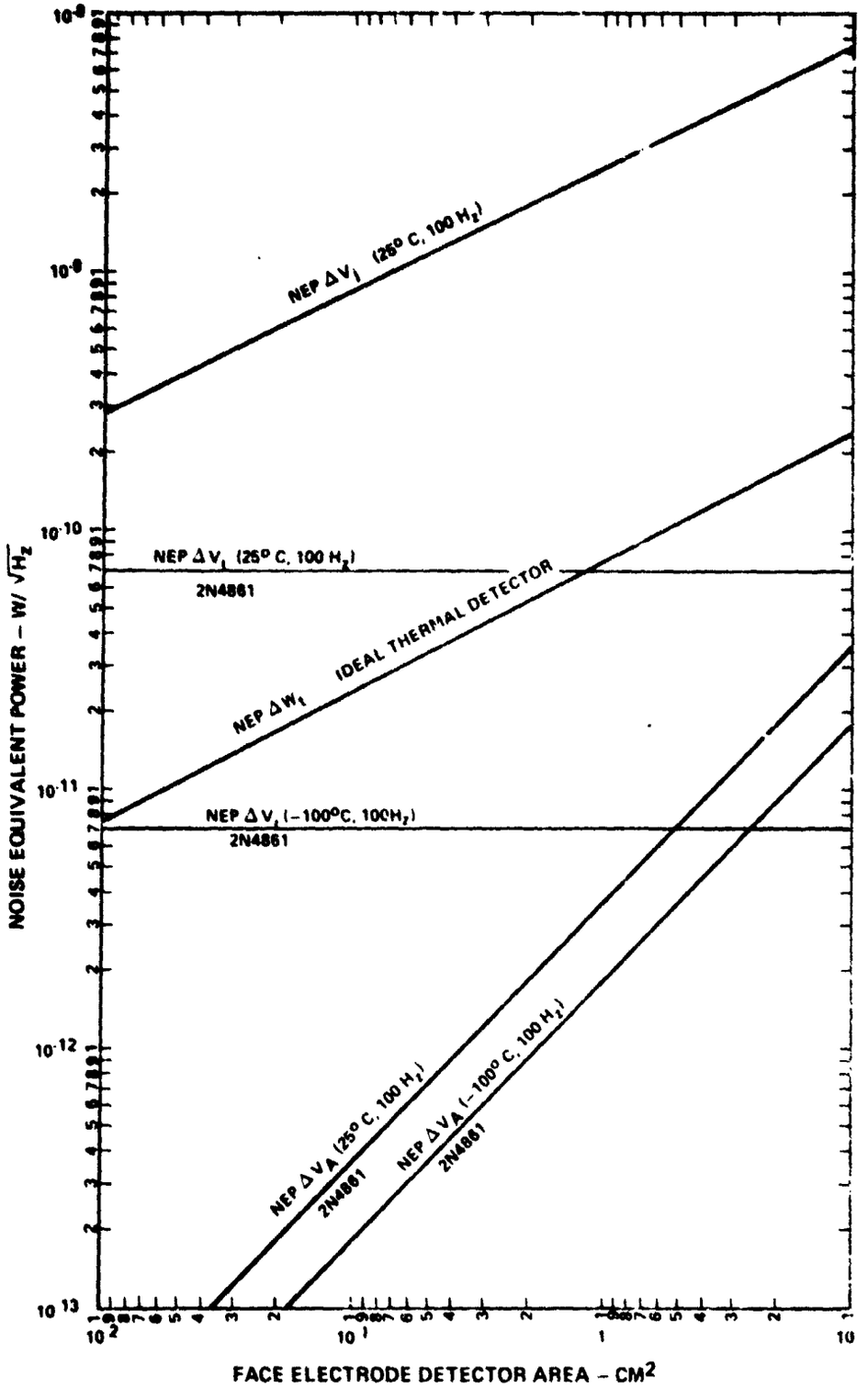

Figure 11. Noise equivalent power of a TGS-based pyroelectric detector as a function of detector area. Amplifier noise is shown for a JFET operated at room temperature and a JFET with cryogenic cooling.

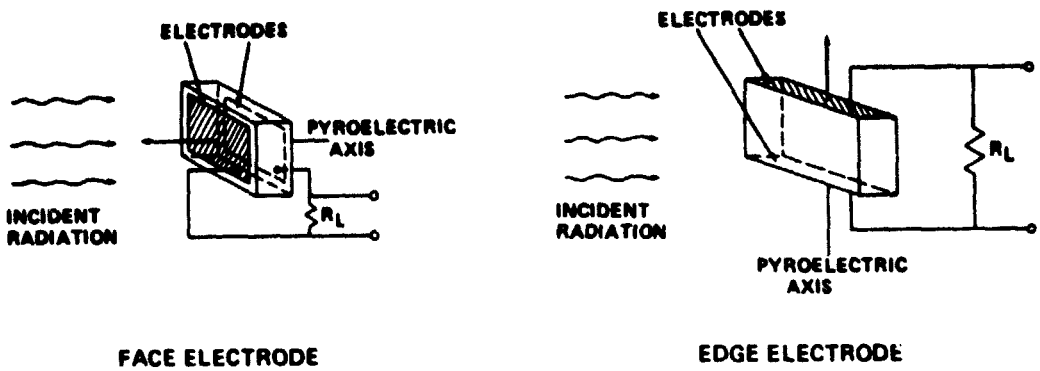

Figure 12. Two possible configurations for a pyroelectric detector element.

SUMMARY

Although photon detectors are the most sensitive infrared detectors available, thermal detectors utilizing the pyroelectric effect have a number of advantages, including broad spectral response, simplicity of construction, ruggedness, and room-temperature operation. These detectors may be optimized for various applications by appropriate choice of element size and shape, absorbing coating, amplifier characteristics and chopping frequency. For example, a simple infrared detector may utilize a small element area, while an infrared imaging system requires a large area. Maximum sensitivity is achieved by maximizing the thermal response of the detector element and by reducing the noise generated in the detector and associated electronics. Maximum thermal response requires a thermal conductance, G, between the detector element and its surroundings approaching the radiative value, a large pyroelectric coefficient λ, and an element emissivity η close to unity. This may be achievable, at least for large area detectors, by improved mechanical design, proper choice of materials, and evacuation of the detector housing. Continuing improvements in JFET characteristics have reduced amplifier noise to such low levels that detector Johnson noise is the primary limitation on detector sensitivity over a wide range of chopping frequencies and element areas. The conductivity of the crystal, which governs the generation of Johnson noise, depends on the concentration and mobility of free charge carriers in the crystal. Since these parameters are probably influenced by the number of defects introduced into the crystal during the growth process, it is reasonable to expect that improvements in the method of growth of TGS crystals will yield crystals with the low conductivities needed to reduce Johnson noise to a value approaching the radiative thermal noise limit.

REFERENCES

1. Matthias, B. T., Miller, C. E., and Remeika, J. P.: Phys. Rev., 104, 849 (1956).

2. Levinstein, H.: Physics Today, 30, No. 11, 23-28 (1977).

3. Gebbie, H. A. et al.: Proc. R. Soc., A20[illegible], 87 (1951).

4. Levinstein, H.: Characterization of Infrared Detectors, Semiconductors and Semimetals (Ed. R. K. Willardson and A. C. Beer), Vol, 5, Academic Press, New York, pp. 3-12, 1970.

5. Kittel, C.: Introduction to Solid State Physics, 2nd ed., Chapter 1, John Wiley & Sons, New York.

6. Curie, J. and Curie, P.: C. R. Acad. Sci. Paris, 91, 294 (1880); Lang, S. B.: Sourcebook of Pyroelectricity, Gordon and Breach Science, London, 1974.

7. Pyroelectricity (temperature-dependent spontaneous electric dipole moment) has been known from ancient times. However, the modern study can be traced back to Gaugain's work in 1856 on such materials as tourmaline. Gaugain, J. M.: C. R. Acad. Sci. Paris, 42, 1264 (1856) and 43, 916 (1856).

8. Lines, M. E. and Glass, A. M.: Principles and Applications of Ferroelectrics and Related Materials, Clarendon Press, Oxford, 1977.

9. Ferroelectricity was first discovered in 1920 by Valasak in Rochelle salt. Valasak, J.: Phys. Rev., 15, 537 (1920) and 17, 475 (1921).

10. Dekker, A. J.: Solid State Physics, Chapter 8, Prentice-Hall, Inc., New York, 1957.

11. Keve, E. T.: Philips Tech. Rev., 35, No. 9, 247-257 (1975).

12. Lock, P. J.: Appl. Phys. Lett., 19, 390 (1971).

13. Keve, E. T.; Bye, K. L.; Whipps, P. W.; and Annis, A. D.: Ferroelectrics 3, 39 (1971).

14. Putley, E. H.: The Pyroelectric Detector, Semiconductors and Semimetals, Vol. 5, Chapter 6 (Ed. R. K. Willardson and A. C. Beer), Academic Press, New York, 1970.

15. Cooper, J.: Rev. Sci. Inst., 33, 92-95 (1962).

16. Cooper, J.: Rev. Sci. Instr., 39. 467-472 (1962).

17. Lang, S. B.: Sourcebook of Pyroelectricity, Gordon & Breach Science, London, 1974. pp. 46-47, 50.

18. Smith, R. A.; Jones, F. E.; and Chasmar, R. P.: The Detection and Measurement of Infrared Radiation, Oxford University Press, London, 1968.

19. Logan, R. M., and Moore, Katharine: Infrared Physics 13, 37-47 (1973).

20. Logan, R. M.: Infrared Physics 13, 91-98 (1973).

21. Baker, G., Charlton, D. E., and Lock, P. J.: Radio Electronic Engr., 42 (6), 260-264 (1972) and Infrared Detectors (Ed. Richard D. Hudson, Jr., and Jacqueline Wordsworth Hudson), Vol. 2, Halsted Press, New York, pp. 240-244.

22. Kennedy, E. J.: University of Tennessee, private communication.

APPENDIX A

THE 32 CRYSTALLOGRAPHIC POINT GROUPS ARRANGED BY CRYSTAL SYSTEMS [8]

Crystal system	Symbol: International	Symbol: Schoenflies	Pyroelectric	Piezoelectric	Centrosymmetric
Triclinic	1	C_1	✓	✓	
	$\bar{1}$	C_i			✓
Tetragonal	4	C_4	✓	✓	
	$\bar{4}$	S_4		✓	
	4/m	C_{4h}			✓
	422	D_4		✓	
	4mm	C_{4v}	✓	✓	
	$\bar{4}$2m	D_{2d}		✓	
	4/mmm	D_{4h}			✓
Hexagonal	6	C_6	✓	✓	
	$\bar{6}$	C_{3h}		✓	
	6/m	C_{6h}			✓
	622	D_6		✓	
	6mm	C_{6v}	✓	✓	
	$\bar{6}$m2	D_{3h}		✓	
	6/mmm	D_{6h}			✓
Monoclinic	2	C_2	✓	✓	
	m	C_s	✓	✓	
	2/m	C_{2h}			✓
Orthorhombic	222	D_2		✓	
	mm2	C_{2v}	✓	✓	
	mmm	D_{2h}			✓
Trigonal	3	C_3	✓	✓	
	$\bar{3}$	S_6			✓
	32	D_3		✓	
	3m	C_{3v}	✓	✓	
	$\bar{3}$m	D_{3d}			✓
Cubic	23	T		✓	
	m3	T_h			✓
	432	O			
	$\bar{4}$3m	T_d		✓	
	m3m	O_h			✓

A tick (✓) indicates that the point group is pyroelectric, piezoelectric, or centrosymmetric, as the case may be.

APPENDIX B

To determine the thermal response of a pyroelectric crystal to a given incident infrared radiation, the following energy balance equation must be solved,

$$\eta W = H \frac{d\theta}{dt} + G\theta \qquad \text{(B-1)}$$

where

η is the emissivity of the crystal detector surface

W is the incident radiation intensity

H is the thermal mass of the crystal detector

G is the thermal conductance between the crystal detector and its heat sink

$\theta = T_d - T$ is the difference in temperature between the crystal detector (T_d) and the heat sink (T)

Because the crystal is a pyroelectric and responds to changes in temperature rather than to a steady state temperature, a mechanical chopper is usually placed in the path of the radiation before it strikes the crystal.

With a chopper of frequency $f = \omega/2\pi$, the form of the radiation which reaches the crystal is

$$W = W_o (1 - e^{i\omega t}) \quad . \qquad \text{(B-2)}$$

The energy balance equation is then written as

$$\eta W_o (1 - e^{i\omega t}) = H \frac{d\theta}{dt} + G\theta \quad . \qquad \text{(B-3)}$$

This is a linear differential equation of order one. The general form of such equations is

$$A(x)\frac{dy}{dx} + B(x)\,y = C(x) \qquad \text{(B-4)}$$

where A, B, and C are functions of x.

To arrive at a solution for this type equation we rearrange terms to get the form

$$dy + P(x)\,y\,dx = Q(x)\,dx \qquad \text{(B-5)}$$

where

$$P(x) = B(x)/A(x)$$

$$Q(x) = C(x)/A(x) \quad .$$

Next we multiply equation (B-5) by $e^{\int P dx}$

$$e^{\int P dx}\,dy + P\,e^{\int P dx}\,y\,dx = e^{\int P dx}\,Q\,dx \quad . \qquad \text{(B-6)}$$

We now show that the left side of equation (B-6) is an exact differential.

$$d\left(ye^{\int P dx}\right) = y\,d\left(e^{\int P dx}\right) + e^{\int P dx}\,dy \qquad \text{(B-7)}$$

and

$$d\left(e^{\int P dx}\right) = \frac{d}{dx}\left(\int P dx\right) e^{\int P dx}\,dx = P\,e^{\int P dx}\,dx \quad . \qquad \text{(B-8)}$$

Then

$$d\left(ye^{\int P dx}\right) = P\,e^{\int P dx}\,y\,dx + e^{\int P dx}\,dy \quad . \qquad \text{(B-9)}$$

We can now rewrite equation (6) as

$$d\left(y\, e^{\int P dx}\right) = e^{\int P dx}\, Q\, dx \quad , \tag{B-10}$$

and solve by direct integration

$$y\, e^{\int P dx} = \int Q\, e^{\int P dx}\, dx \quad . \tag{B-11}$$

We now apply the preceding method to equation (3). First, we rearrange terms to give

$$d\theta + \frac{G}{H}\,\theta\, dt = \frac{\eta W_o}{H}\,(1 - e^{i\omega t})\, dt. \tag{B-12}$$

Next, we multiply equation (12) by the integrating factor $e^{\int \frac{G}{H} dt}$

$$e^{\int \frac{G}{H} dt}\, d\theta + e^{\int \frac{G}{H} dt}\, \frac{G}{H}\,\theta\, dt = e^{\int \frac{G}{H} dt}\, \frac{\eta W_o}{H}\,(1 - e^{i\omega t})\, dt \quad . \tag{B-13}$$

We then integrate equation (13)

$$\theta\, e^{\frac{G}{H} t} = \frac{\eta W_o}{H} \int e^{\frac{G}{H} t}\,(1 - e^{i\omega t})\, dt \tag{B-14}$$

$$\theta = \frac{\eta W_o}{H}\, e^{-\frac{G}{H} t}\left[\int e^{\frac{G}{H} t}\, dt - \int e^{\left(\frac{G}{H} + i\omega\right) t}\, dt\right] \tag{B-15}$$

$$\theta = \frac{\eta W_o}{H}\, e^{-\frac{G}{H} t}\left[\frac{1}{G/H}\, e^{\frac{G}{H} t} - \frac{1}{(G/H + i\omega)}\, e^{\left(\frac{G}{H} + i\omega\right) t} + C\right] \tag{B-16}$$

$$\theta = \frac{\eta W_o}{G} - \frac{\eta W_o}{(G + i\omega H)}\, e^{i\omega t} + C' e^{-\frac{G}{H} t} \quad . \tag{B-17}$$

The initial conditions are $\theta = 0$ when $t = 0$. Solve (17) for the constant of integration c'

$$0 = \frac{\eta W_o}{G} - \frac{\eta W_o}{(G + i\omega H)} + C'$$

$$C' = \frac{-\eta W_o}{G} + \frac{\eta W_o}{(G + i\omega H)} \quad . \tag{B-18}$$

Substituting for c' in equation (17) gives

$$\theta = \frac{\eta W_o}{G}\left(1 - e^{-\frac{G}{H}t}\right) - \frac{\eta W_o}{G + i\omega H}\left(e^{i\omega t} - e^{-\frac{G}{H}t}\right) \quad . \tag{B-19}$$

This is the solution to equation (B-1). However, it is instructive to put this solution in a somewhat different form. Consider the term

$$\frac{\eta W_o}{G + i\omega H}\, e^{i\omega t} = \frac{\eta W_o}{G + i\omega H}\,\frac{G - i\omega H}{G - i\omega H}\, e^{i\omega t} = \frac{\eta W_o}{G^2 + \omega^2 H^2}\,(G - i\omega H)\, e^{i\omega H} \quad . \tag{B-20}$$

Now

$$(G - i\omega H)\, e^{i\omega t} = (G - i\omega H)\,(\cos \omega t + i \sin \omega t) \tag{B-21}$$

$$= G \cos \omega t - i\omega H \cos \omega t + i\, G \sin \omega t + \omega H \sin \omega t \tag{B-22}$$

$$= [G \cos \omega t + \omega H \sin \omega t] + i\,[G \sin \omega t - \omega H \cos \omega t] \quad . \tag{B-23}$$

Let

$$G = \cos \phi \text{ and } \omega H = \sin \phi \quad . \tag{B-24}$$

then

$$(G - i\ H)\ e^{i\omega t} = [\cos\ \omega t \cos\ \phi + \sin\ \omega t \sin\ \phi]$$

$$+ i\ [\sin\ \omega t \cos\ \phi - \cos\ \omega t \sin\ \phi]$$

$$= \cos\ (\omega t - \phi) + i \sin\ (\omega t - \phi) \qquad \text{(B-26)}$$

$$= e^{i\ (\omega t\ -\ \phi)} \text{ where } \tan\ \phi = \frac{\omega H}{G} \qquad \text{(B-27)}$$

Equation (19) can then be written in the following form:

$$\theta = \frac{\eta W_o}{G}\left(1 - e^{-\frac{G}{H}t}\right) - \frac{\eta W_o}{(G^2 + \omega^2 H^2)}\ e^{i(\omega t\ -\ \phi)} \quad , \qquad \text{(B-29)}$$

where the terms on the right-hand side are the steady state, transient and oscillatory terms, respectively.

APPROVAL

THE PYROELECTRIC PROPERTIES OF TGS FOR APPLICATION IN INFRARED DETECTION

By R. L. Kroes and D. Reiss

The information in this report has been reviewed for technical content. Review of any information concerning Department of Defense or nuclear energy activities or programs has been made by the MSFC Security Classification Officer. This report, in its entirety, has been determined to be unclassified.

Lewis L Lacy

LEWIS L. LACY
Chief, Solid State Branch

Robert J Naumann

ROBERT J. NAUMANN
Chief, Space Processing Division

Charles A. Lundquist

CHARLES A. LUNDQUIST
Director, Space Sciences Laboratory

☆U S GOVERNMENT PRINTING OFFICE 1980 -740-066/294 REGION